Hindawi
Shock and Vibration
Volume 2021, Article ID 2764803, 12 pages
https://doi.org/10.1155/2021/2764803

Research Article

Experimental Study on the Transition between Static and Kinetic Frictions of Steel/Shale Pairs

Qin Lian,[1] **Chunxu Yang**,[1] **and Jifei Cao**[2]

[1]*Technical Development Department, Sinopec Shengli Petroleum Engineering Co., Ltd., Dongying 25700, China*
[2]*Drilling Technology Research Institute, Sinopec Shengli Petroleum Engineering Co., Ltd., Dongying 25700, China*

Correspondence should be addressed to Chunxu Yang; spring.sun@163.com

Received 13 September 2021; Accepted 6 October 2021; Published 11 November 2021

Academic Editor: Peng Wang

The transition between static and kinetic frictions of steel/shale pairs has been studied. It was found that the coefficient of friction decreased exponentially from static to dynamic friction coefficient with increasing sliding displacement. The difference between static and dynamic friction coefficients and the critical distance D_c under the dry friction condition is much larger than that under the lubricated condition. The transition from static to dynamic friction coefficient is greatly affected by the normal load, quiescent time, and sliding velocity, especially the lubricating condition. Maintaining continuous lubrication of the contact area by the lubricant is crucial to reduce or eliminate the stick-slip motion. The results provide an insight into the transition from static to dynamic friction of steel/shale pairs.

1. Introduction

Slide drilling with a bent-housing motor dominates the directional market of the petroleum and natural gas drilling industry [1]. The drill string with a length of thousands of meters slides along the axial direction inside the cylindrical borehole wall at a very low speed (0.1–1 mm/s); at the same time, stick-slip between the drill string and borehole wall occurs frequently due to the transition between static and kinetic frictions and the velocity weakening of the friction coefficient. The friction model which only considers a constant dynamic friction coefficient (such as the Coulomb model) used for rotary drilling is inapplicable in slide drilling. On the contrary, the accurate value of friction force between the drill string and borehole wall under the sliding drilling condition is the basis data for designs of well track and tool face adjusting and is the bond between data at the wellhead and bottom of the well, which is also the key issue to realize intelligent drilling [2, 3]. Thus, the friction coefficient between the drill string and borehole wall is a new and very important problem that needs to be resolved immediately.

A number of studies on stick-slip motion in a low-velocity regime, caused by the time dependence of static friction, the transition between static and kinetic frictions, and the velocity weakening of the friction coefficient, have been carried out. Several friction models have been formulated in terms of friction coefficients as a function of the relative sliding velocity, displacement, and quiescent time [4–13], which can be categorized as physics-based [14–17] and phenomenological [18–21]. Phenomenological friction models include static [18] and dynamic models [22–24]. Static models are usually described as a function of relative velocity, such as the well-known Coulomb and Stribeck models, and can capture the drooping characteristic but hysteretic behavior of the friction force. The friction force of dynamic models depends on internal states along with the relative velocity of the contacting surfaces, such as the well-known Dahl [25] and RSF (rate and state friction) models, and can capture hysteretic behaviors of the friction force at the same time. In particular, RSF model has been very successful in describing macroscale friction for many materials, including rocks [26–31]. In the petroleum and natural gas drilling industry, Coulomb friction model was adopted to calculate the friction force between the drill string and borehole wall in the last few decades, and the Stribeck model [32], Dahl model [33], and self-contained friction model [34] were used with the application of technology of

friction reduction by vibrating the drill string until a few years ago. The introduction of these models considers the effect of stick-slip motion of the drill string on friction to a certain extent; however, the characteristics of low velocity, stick-slip, and complex lubricating condition of the relative motion between the drill string and borehole wall make it difficult for the friction model related to velocity and quiescent time to play a role, and the more complex the model is, the more difficult it is to identify its parameters. The friction model, as a function of the relative sliding displacement, is more suitable for the operating condition in the petroleum and natural gas drilling industry.

The critical distance (D_c) is understood to be the elastic deformation necessary to break the contact between asperities, formed during static contact of the interface materials, where the static friction coefficient persists before it steadily decreases to the kinetic one [35], and varies for different rubbing pairs [36, 37]. Tian et al. [38] carried out nanoscale experiment to account for the activation and passivation of chemical reaction sites and the formation of new chemical bonds from dangling bonds during sliding, and results showed D_c is sensitive to the surface chemistry and nearly independent of sliding velocity. Li et al. [39] performed aging experiments for single-asperity silica-silica nanocontacts to isolate the physical mechanisms and found the static friction increased logarithmically with time for hold times from 0.1 to 100 s in the absence of plastic deformation of the contact, which strongly supported chemical bond formation as the operative aging mechanism. Mitchell et al. [37] investigated the frictional properties of gabbro under low normal stress, dry, and hydrated conditions and found that slip becomes increasingly more unstable (velocity weakening) with increasing temperature. Thus, the transition from static to dynamic friction coefficient and the critical distance for different rubbing pairs are influenced by many factors and difficult to be determined by the theoretical arithmetic.

The aim of the present paper was to study the transition law from static to kinetic friction and the critical distance of steel/shale pairs under unlubricated or oil-lubricated conditions. This paper is organized as follows: the setup and procedure of the experiment are described in Section 2, and the surface morphology and mechanical parameters of the steel/shale pair were measured through the nanometer indentation method. The effects of normal load, quiescent time, sliding velocity, and lubricated condition on the transition from static to dynamic friction coefficient are shown and analyzed in Section 3. The microscopic wear and materials' transfer of the steel/shale specimens are, respectively, scanned and measured in Section 4 to analyze the reason for the transition between static and dynamic frictions.

2. Experimental Details

2.1. Setup and Procedure. The coefficients of static and dynamic frictions and their transition were measured by using a specially designed ball-on-rectangular solid friction tester shown in Figure 1. The steel ball (13 mm-diameter balls of 35CrMo) and shale were used as the sliders in the tribological tests. The shale specimens were collected from an outcrop of the Lower Silurian Longmaxi Formation at the Sichuan Basin in southwestern China, which is the most significant exploration area for unconventional gas in China. The steel ball specimen was attached to a rigid square box and pressed by dead weights of 22 or 38 N, respectively, against the rectangular solid shale specimen. The tangential force (F_T) acquisition began after applying the normal load, and the steel ball slid along the axial direction of the screw rod with speed V until the terminal of single trip and slid backward after resting for 0, 1, 5, 30, and 60 s, respectively. Repeat this process until the experimental set time was over. From the resulting F_T versus time, the static coefficient of friction μ_s was determined as the ratio of tangential force at the onset of relative sliding divided by the applied normal load. After the transition from static to kinetic friction, relative sliding occurred generally with the velocity of 22.78, 85.72, and 266.67 μm/s, respectively. The kinetic coefficient of friction μ_k was determined as the ratio of tangential force at the steady relative sliding divided by the applied normal load. For more details about the experimental setup, refer to [40].

Before each test, the specimens were cleaned in an ultrasonic bath with isopropanol. Unlubricated tests were run in the laboratory air at a room temperature of 20°C and the relative humidity of 64%. In the lubricated tests, additive-free mineral oil was fed into the contact area before the ball and the plate were mated, and the viscosity of oil is $\eta_{20°C} = 0.294$ Pa·s and $\eta_{40°C} = 0.085$ Pa·s.

2.2. Materials. In order to obtain the surface quality of specimens, white light interferometry and electron microscope scanning were conducted for the commercially available steel ball and the polished shale before tests. The shale specimens were finished by sandpaper with 400, 1200, and 3000 meshes under a normal force of 10 N during 20 s, respectively. The roughness value R_a of the steel ball equals 0.20 μm. Figure 2 shows the scanning electron micrographs of three shale surfaces. The surface morphology parameters of the shale samples, including R_a (arithmetic average roughness), R_{pk} (height and portion of asperity peaks), and R_k and R_{vk} (depth and portion of cavities on the machined surface, respectively), before tests are shown in Table 1.

The contact between the real rough surface is usually a mixed elastoplastic system. The plasticity index, ψ, was computed for both contacting surfaces in order to describe the deformation properties of the contacting asperities. Whitehouse [41] proposed a plasticity index defined by

$$\psi = \frac{E'}{H}\sqrt{\frac{R_q}{R}}, \tag{1}$$

$$\frac{1}{E'} = \frac{1-\nu_1^2}{E_1} + \frac{1-\nu_2^2}{E_2}, \tag{2}$$

where ψ is the plasticity index, the contact deformation is fully elastic when $\psi < 0.6$, fully plastic when $\psi > 10$, and elastoplastic when $1 < \psi < 10$; E' is the composite modulus of elasticity, MPa; H is the Brinell hardness of materials, MPa; R_q is the root-mean-square roughness of surface asperities,

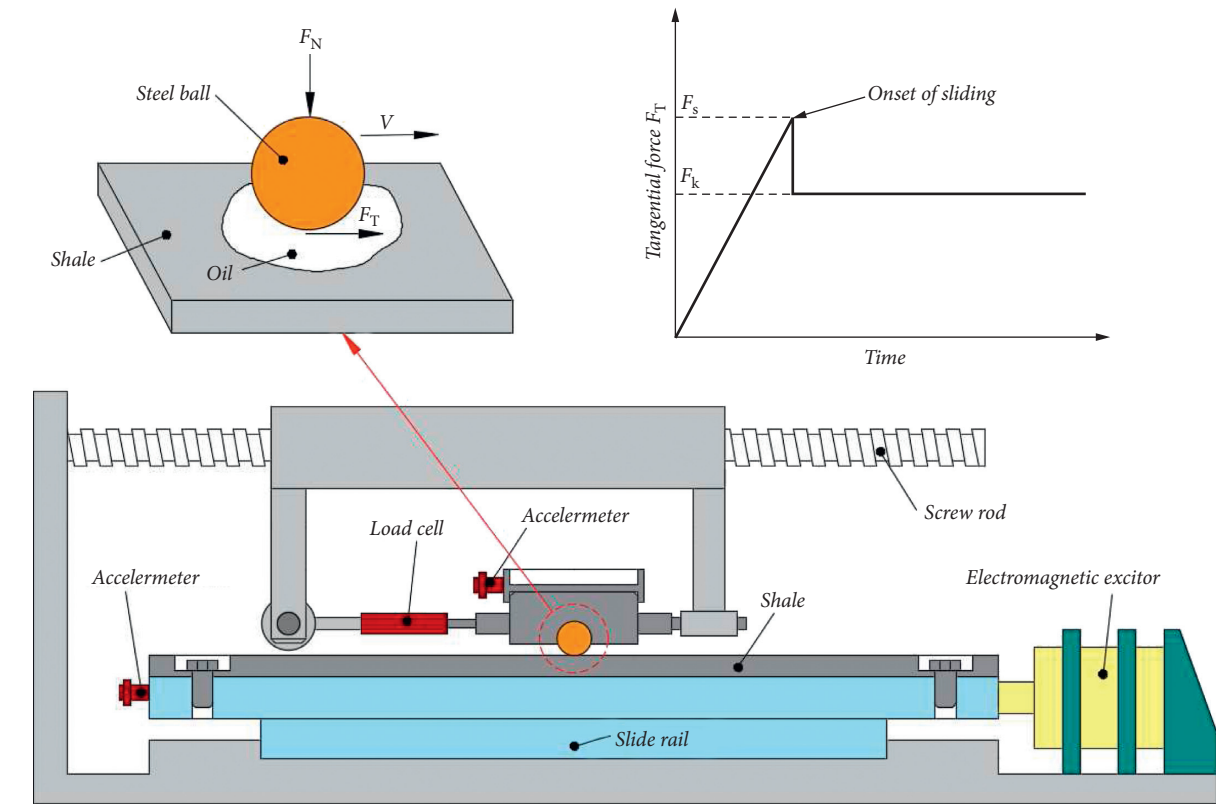

Figure 1: Experimental setup and a hypothetical static to kinetic friction transition diagram.

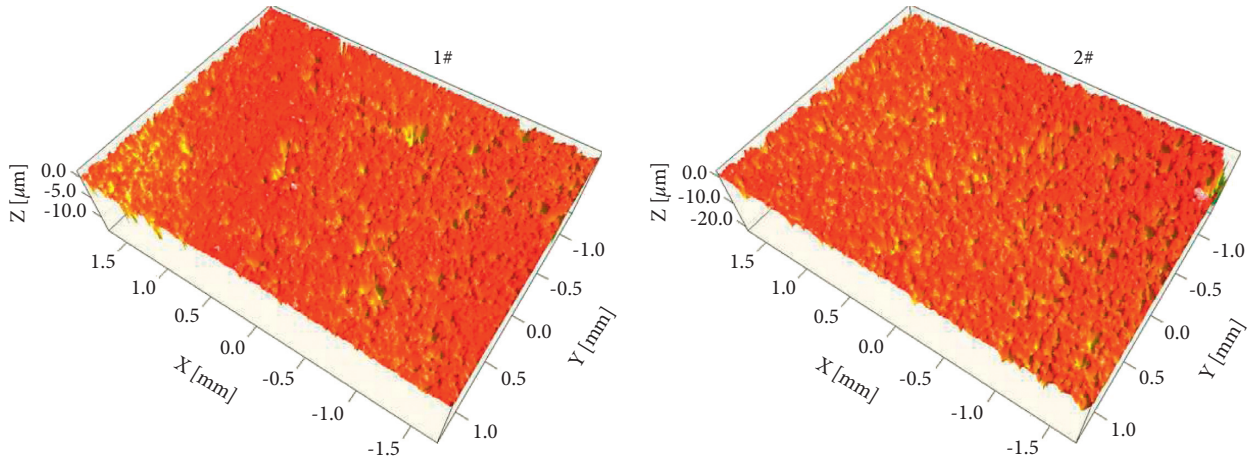

Figure 2: Continued.

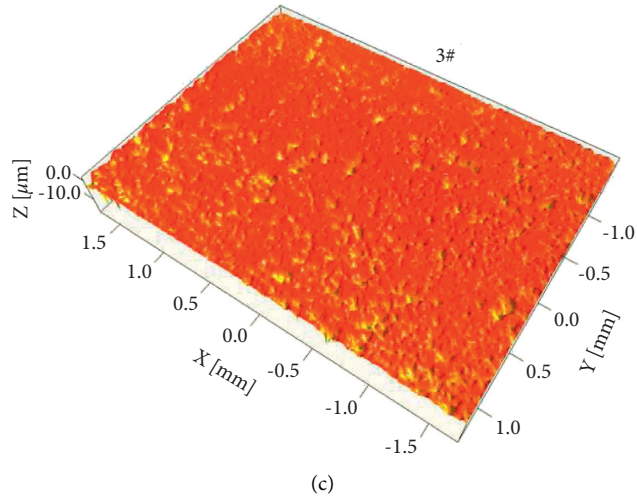

(c)

Figure 2: SEM micrographs of shale surfaces.

Table 1: Values of the surface morphology parameters of the shale specimen.

Roughness parameter (μm)	Shale 1#	Shale 2#	Shale 3#
R_a (arithmetic surface roughness value)	0.491	0.740	0.421
R_q (root-mean-square roughness)	0.693	0.944	0.622
R_k (core roughness depth)	1.011	1.667	0.970
R_{pk} (reduced peak height)	0.200	0.399	0.238
R_{vk} (reduced valley depth)	1.307	1.673	1.266

μm; R is the radius of curvature of asperities, $R = 8$ (when $R_a = 0.7$–0.8) or 12 (when $R_a = 0.4$–0.5), μm; E_1 and E_2 are Young's modulus of the steel ball and shale, respectively, MPa; and ν_1 and ν_2 are the Poisson ratio of the steel ball and shale, respectively.

The dot matrix nanoindentation method [42] was adopted to obtain the mechanical properties of the shale specimen, such as Young's modulus, hardness, and Poisson's ratio. The indenter gradually pressed into the shale specimen, the material near the pressure head first generated elastic deformation and changed to plastic deformation with the increase of load, and an indentation matching the shape of the indenter appeared in the sample. When the indenter was unloaded, the elastic deformation was restored, while the plastic deformation formed the indentation crack (see Figure 3). The load-displacement curve of the nanoindentation was drawn based on the experimental data, based on which Young's modulus and hardness of the shale were calculated. Substituting the surface morphology and mechanical parameters of steel/shale specimens measured into equations (1) and (2), the plasticity of the steel ball/shale pairs could be obtained, as shown in Table 2. From these values of the plasticity index, it can be concluded that both elastic and plastic deformations exist simultaneously.

3. Results

3.1. Friction Coefficient Change during Motion Restart. Figure 4 shows the change of frictional coefficient in the restarting process after 30 seconds of motionless. From Figures 4(a) and 4(b), the frictional coefficient first increases linearly to the maximum (i.e., the static friction) and then decreases exponentially to a steady value (i.e., the dynamic friction) with increasing sliding displacement in one sliding period under dry friction conditions, and the change laws of friction coefficient in the two sliding periods are almost the same, which means that the friction coefficient changes significantly in the transition process between motionless and sliding. From Figures 4(c) and 4(d), the static friction coefficient is significantly reduced, and there is no obvious transition between static and dynamic friction coefficients under lubricated conditions. The fluctuation of the frictional coefficient is due to the instability of the lubrication state between the contact surfaces.

3.2. Effect of Quiescent Time and Sliding Velocity. The effect of the quiescent time and sliding velocity on the transition from static to kinetic friction was studied under unlubricated and lubricated conditions. Figure 5 shows the effect of quiescent time on the friction coefficient measured on steel/shale under different normal loads and lubricating conditions. The static and kinetic friction coefficients were determined as the ratio of tangential force F_T at the peak and steady values divided by the applied normal load, respectively. When the steel ball began to slide, the tangential force increased almost linearly up to peak, and onset of the first slip was accompanied by a discontinuity in the course of F_T versus time. After the frictional coefficient reaches its maximum in the condition of dry friction, the frictional coefficient under higher normal load drops sharply to the kinetic friction coefficient, while this

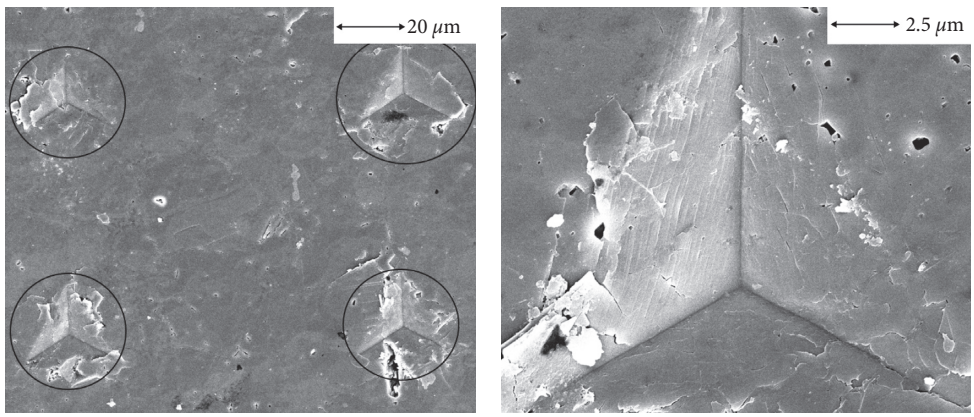

Figure 3: SEM pictures of indentation. (a) Dot matrix. (b) Single.

Table 2: Mechanical parameters and plasticity index of steel/shale specimens.

Mechanical parameter	Steel ball	Shale 1#	Shale 2#	Shale 3#
E (GPa)	190		44.41	
ν	0.305		0.24	
(GPa)	1.0097		2.64	
R_q (μm)	0.28	0.693	0.944	0.622
R (μm)	20	12	8	12
ψ	4.51	3.50	5.00	3.32

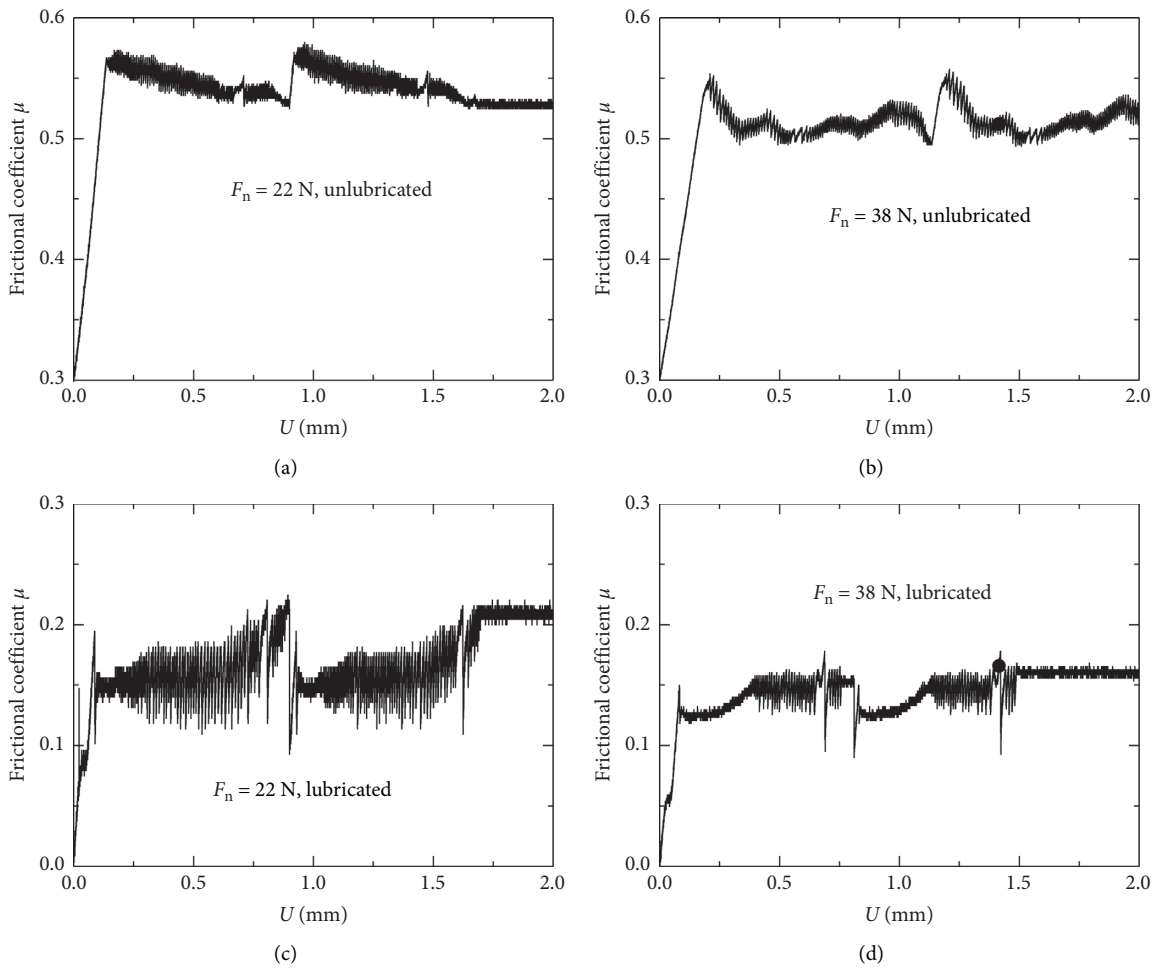

Figure 4: The friction coefficient during motion restart (V = 22.78 μm/s and quiescent time equals 30 s).

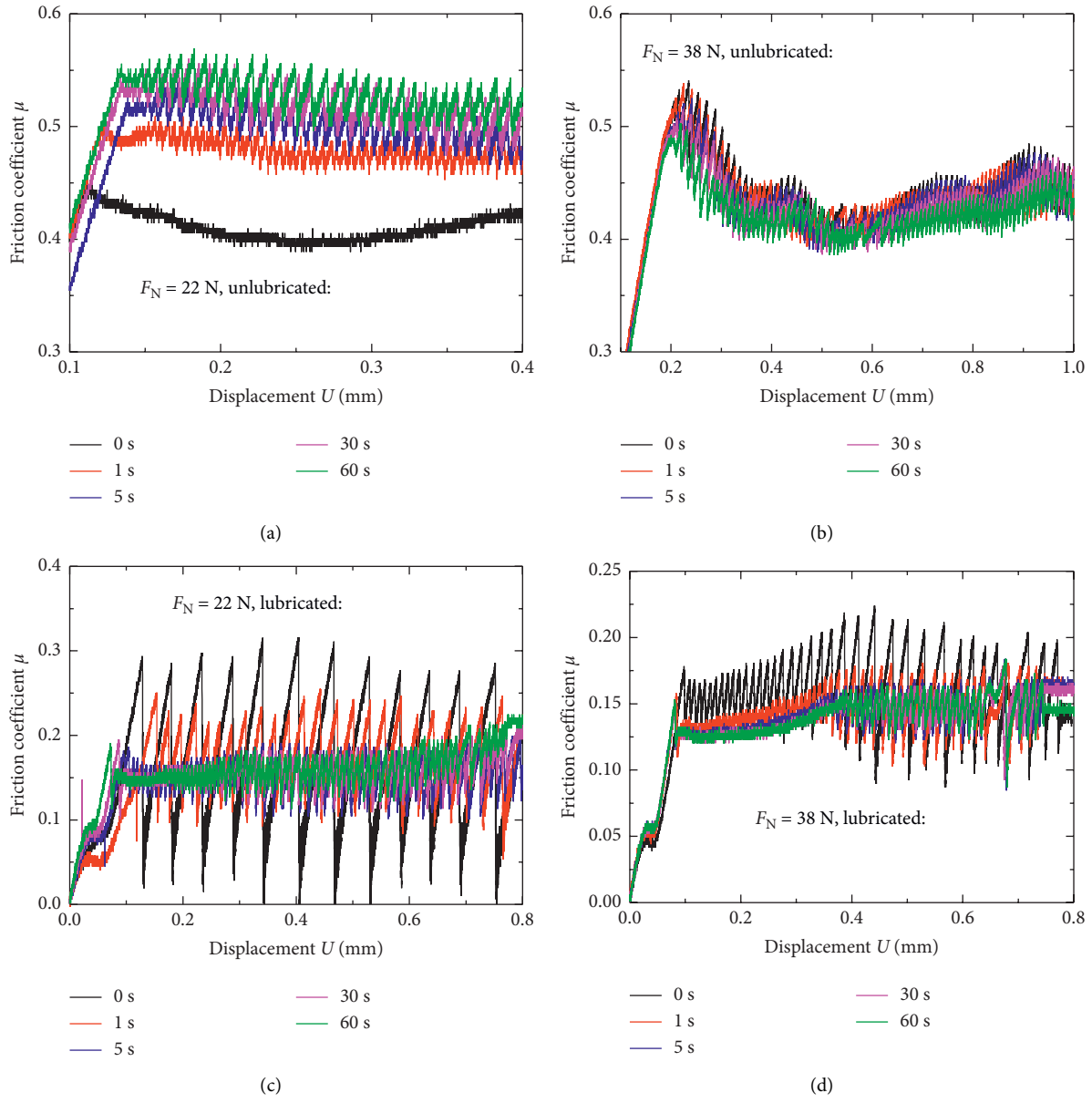

Figure 5: Effect of quiescent time on the transition from static to kinetic friction ($V = 22.78\mu m/s$).

process becomes very gentle under lower normal load. Under the lubricated condition, the average value of friction coefficient decreases significantly and fluctuates acutely compared with the unlubricated condition, and the boundary between static friction and dynamic friction becomes blurred. The quiescent time (from 0 to 60 s) between the adjacent sliding period had small effect on the average value of coefficient of friction for the unlubricated condition while larger effect for the lubricated condition. This may attribute to the influence of quiescent time on the distribution of lubricating oil. Larger quiescent time was beneficial to oil entering into the interface of rubbing pairs again where oil has been extruded in the preceding motion.

Figure 6 shows the effect of sliding velocity on the transition from static to kinetic friction under different normal loads. It can be seen that the average frictional coefficient increases (especially in higher normal load) with increasing sliding velocity, and the stick-slip motion intensifies which makes the transition between static and kinetic friction coefficients become indistinct. The main reason for the above phenomenon is that the higher sliding speed extrudes lubricating oil from the contact interface, resulting in an increase in the average friction coefficient. At the same time, the deterioration of lubrication conditions intensifies the stick-slip movement.

3.3. Transition from Static to Kinetic Friction. The following law was determined to model the transition from static to dynamic friction coefficient [12]:

$$\mu = \mu_d + (\mu_s - \mu_d)e^{-Cq}, \tag{3}$$

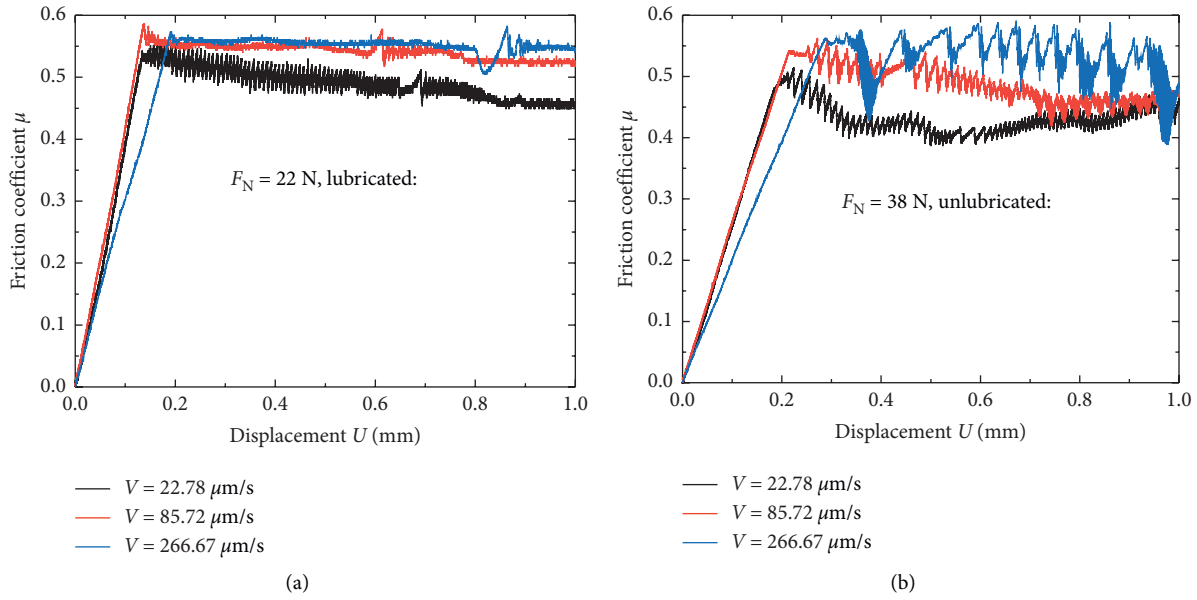

Figure 6: Effect of sliding velocity on the transition from static to kinetic friction.

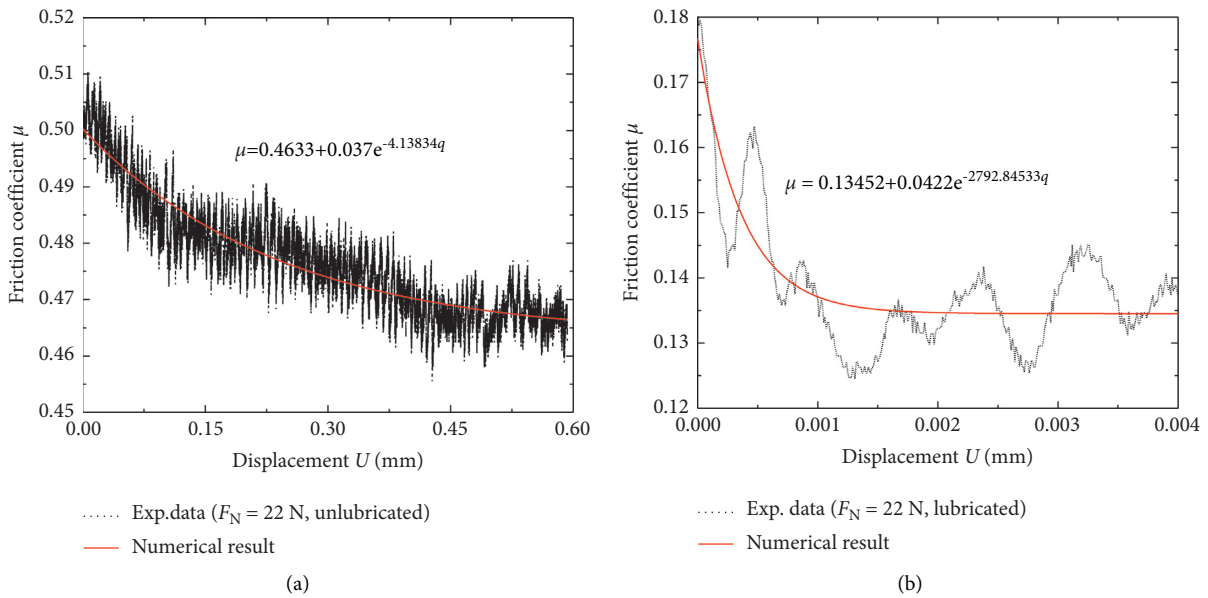

Figure 7: Continued.

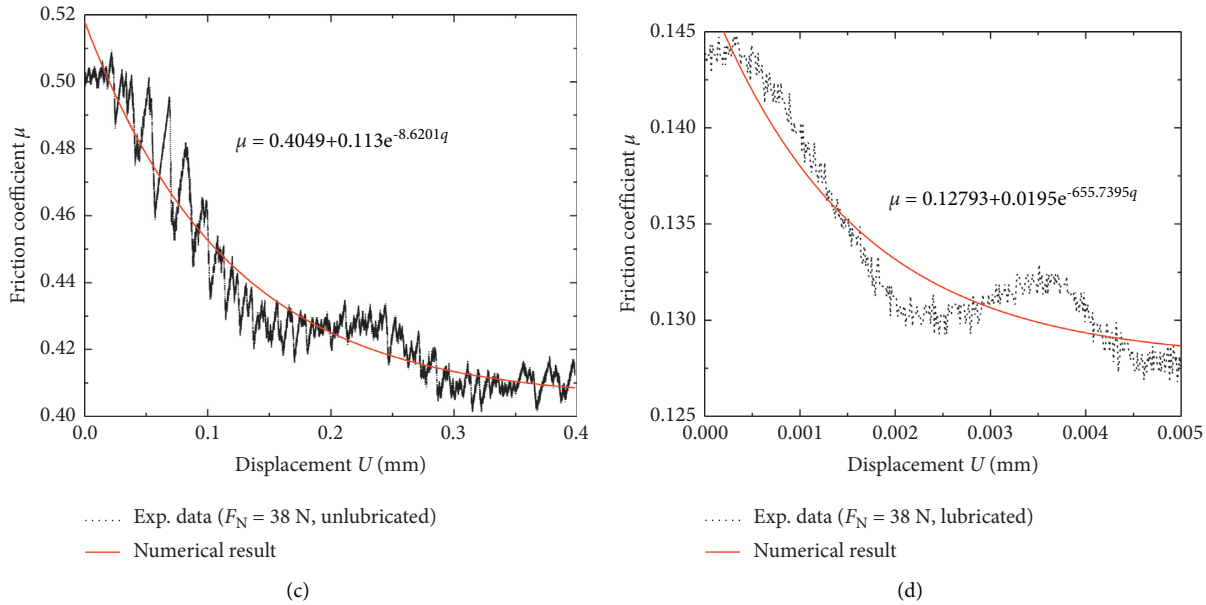

Figure 7: Fitting of the friction coefficient versus displacement ($V = 22.78\mu$m/s).

where q is the sliding distance, mm; C is a constant that determines the convergence rate; μ_d is the dynamic friction coefficient; and μ_s is the static friction coefficient.

Figure 7 shows the fitting results of the friction coefficient transition from static to kinetic friction using equation (3). It can be seen that the average friction coefficients decreased exponentially with increasing sliding displacement under both unlubricated and lubricated conditions. The difference between static and kinetic friction coefficients under the lubricated condition became smaller.

As the friction coefficients fluctuated sharply and depended on the quality of surfaces strongly under a higher sliding velocity, the experimental data of low sliding velocity ($V = 22.78\mu$m/s) in Figure 7 are chosen to analyze the critical distance D_c, which is the length to break the contact between asperities, leading to a continuous decrease of the friction coefficient until the kinetic value is reached. The calculated results of critical distance D_c for steel/shale pairs were compared with other materials [43], as shown in Figure 8. It can be seen that the critical distance D_c of steel/shale pairs under the lubricated condition is much smaller than that under the unlubricated condition and is close to the critical distance of metal materials while lower than the soft materials (such as acrylic or wood) (see Table 3). D_c decreases with increasing normal load under the dry friction condition, and D_c of the lubricated condition is much smaller than that of the dry friction condition, and the values of D_c are similar under different normal loads, which is consistent with the experimental results in the related literature [37].

4. Discussion

Normal load, quiescent time, sliding velocity, and lubrication influenced the static friction and transition from static to kinetic friction at the operating conditions used in this study. The static coefficient of friction of both unlubricated and lubricated pairs decreased with increasing normal load. The difference between static and dynamic coefficients increased with increasing normal load under the unlubricated condition, while its value changed little under the lubricated condition. The quiescent time influenced the friction coefficients a lot under low normal load while little under higher normal load. Under the condition of oil-free lubrication, the static friction coefficient increases with increasing sliding speed, and the transition from static to kinetic friction coefficients basically disappears.

Figure 9 shows the fiction coefficient measured under the unlubricated condition under the normal load of 38 N versus sliding displacement and the SEM micrographs of the friction track on the shale specimen. At the place of onset of first sliding, the friction force increased to the static friction coefficient (point 2, Figure 9(a)) owing to penetration of roughness peaks of the shale into the surface of the steel ball, and the surface showed white curve areas accordingly (Figure 9(b)) which revealed plastic deformation and shale broken, and several light white-banded scratches on the right of point 2 were also observed inside the friction track. When the tangential force overcomes the resistance to abrasive grooving of the steel surface and shear strength of shale (point 2), the static friction coefficient decreases to kinetic friction coefficient (point 3). From point 1 to point 3, the broken areas of the shale surface (white areas) increase first and then decrease and remain stable during subsequent sliding. The transition from the higher static to the lower kinetic friction coefficient with the steel/shale pair can be explained by the rupture of asperities of shale surfaces. Figure 10 shows the enlarged view of area between point 1 and point 2 with different magnification times shown in Figure 9(b); it can be seen that the area is low-lying, and a large number of broken mineral particles still attach to the

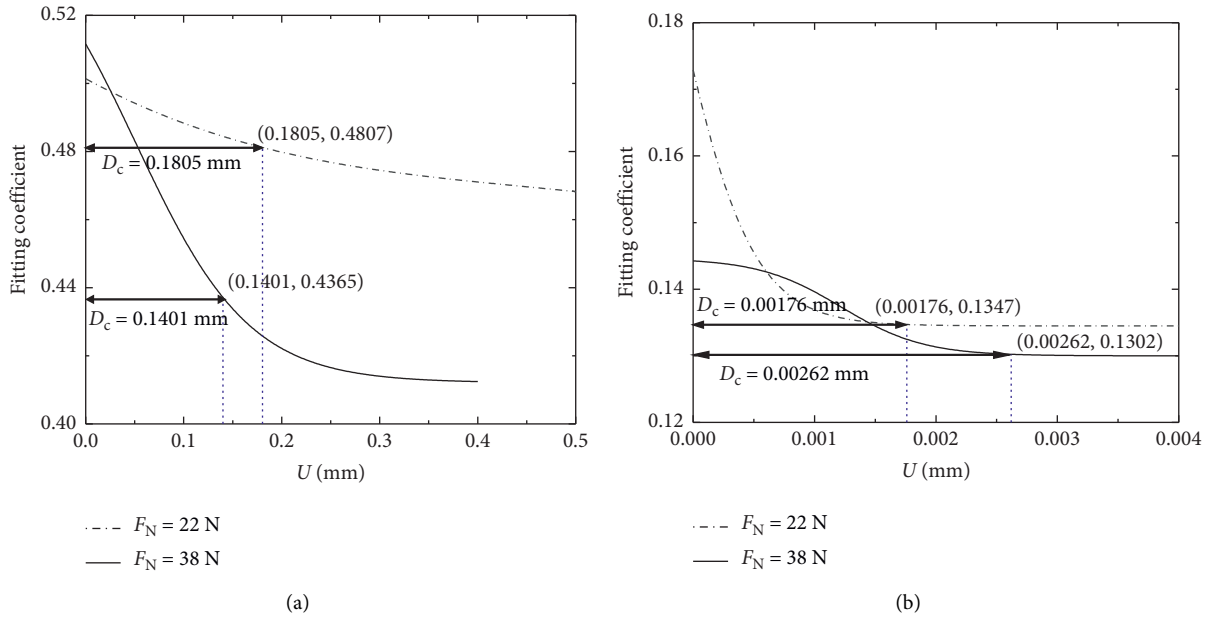

FIGURE 8: Average friction coefficient μ versus displacement U and the estimated D_c (V = 22.78μm/s). (a) Unlubricated. (b) Lubricated.

TABLE 3: Values of D_c for different materials [36, 38].

Materials	Un-/lubricated	μ_s	μ_k	D_c (μm)	Ref.
Mild steel on copper	Unlubricated	0.54	0.39	0.9	Rabinowicz, [35]
	Lubricated	0.58	0.40	0.7	
Mild steel on titanium	Unlubricated	0.63	0.45	6.0	
	Lubricated	0.61	0.45	5.0	
Acrylic on wood	Unlubricated	0.3	0.06	290.0	Mendez and Miguel [36]
Wood on wood	Unlubricated	0.2	0.07	420.0	
Steel on shale	Unlubricated	0.51	0.41	160.3	This paper
	Lubricated	0.144	0.13	2.19	

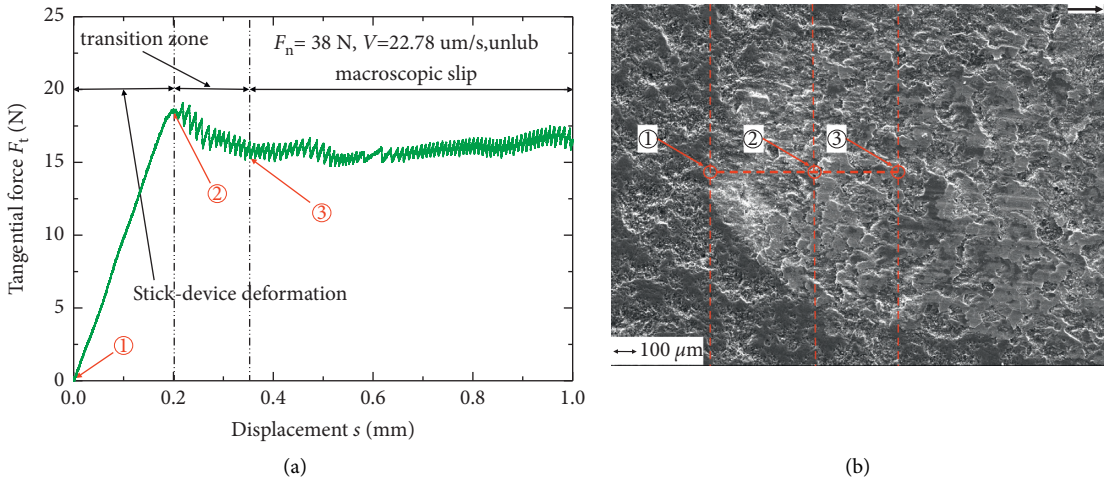

FIGURE 9: Tangential force measured on the unlubricated mild steel/shale pair versus time of testing. SEM micrographs of the contact area of the shale after different times of testing (arrows indicate the direction of tangential force applied).

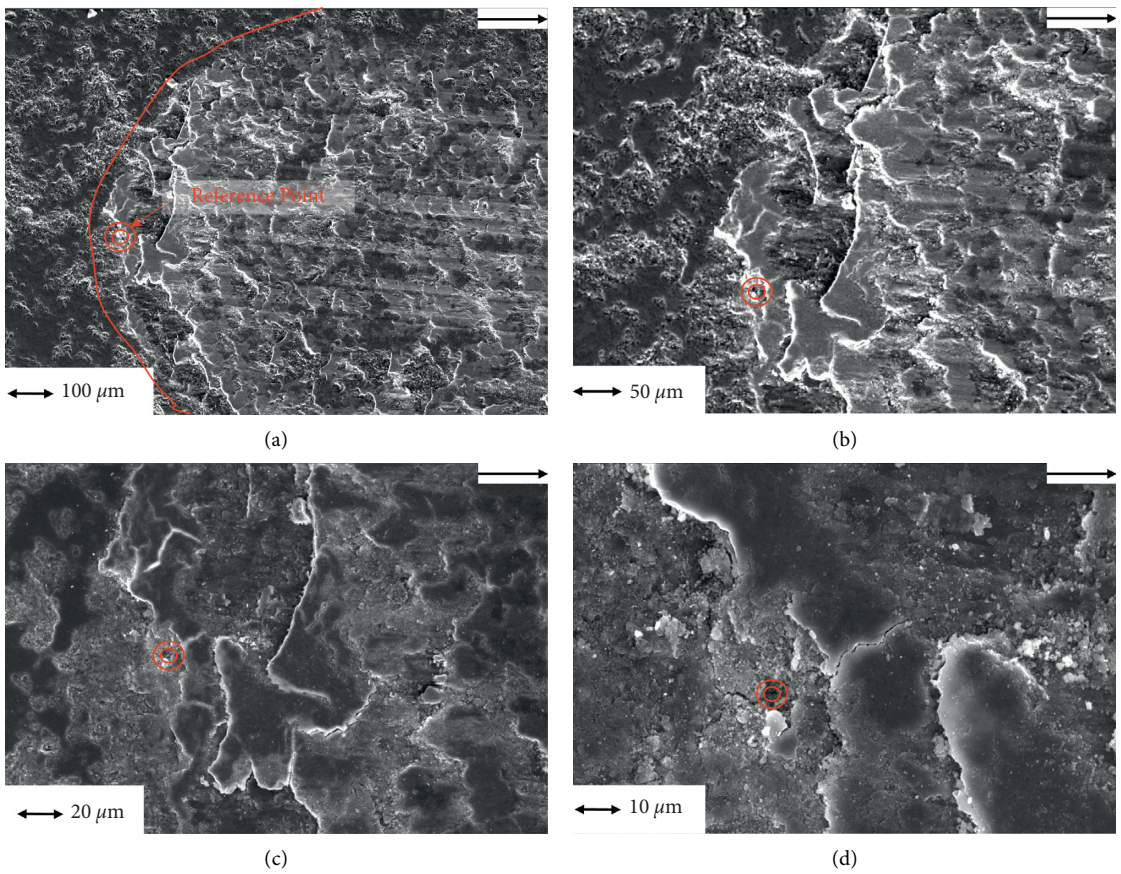

Figure 10: SEM micrographs of the shale surface at the area of first sliding (arrows show the direction of relative sliding). (a) ×100. (b) ×200. (c) ×300. (d) ×1000.

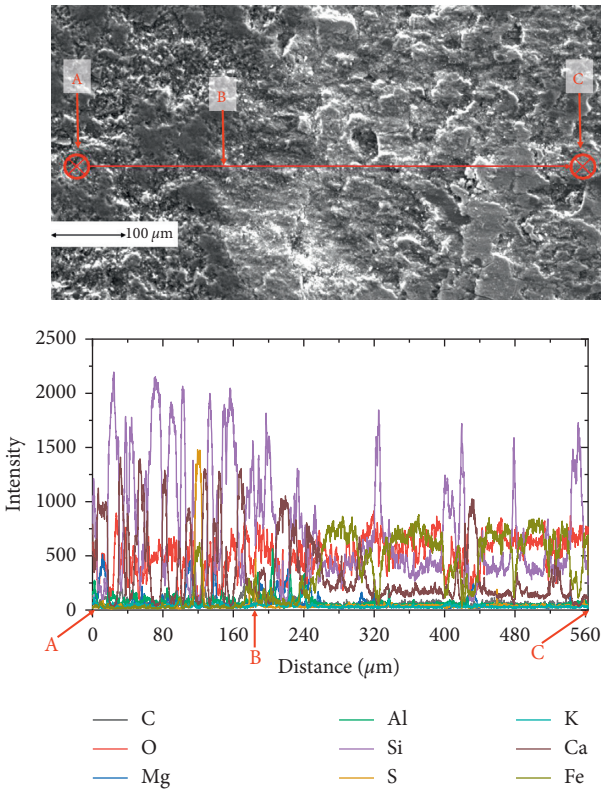

Figure 11: The material transfer between the steel ball and shale.

shale surface although the surface has been cleaned up before scanning.

Material transfer from the steel ball was detected on the contact surface of the shale specimen (Figure 11). Starting from the boundary of the scratch (point B), the proportion of Si and Ca elements decreases significantly, while that of the Fe element increases significantly. It indicates that the quartz minerals (Si element based), calcite, and dolomite (Ca element based) in the shale surface decrease after friction tests, which may be embedded in the steel ball surface or fractured and removed. At the same time, portion of the Fe element of the steel ball transfers to the shale surface. Transition behavior was changed, and kinetic friction of the steel/steel pairs was remarkably reduced by oil lubrication in this paper. Stick-slip effects (Figures 5(c) and 5(d)) occurred on the lubricated steel/shale pairs. This was attributed to squeezing out of oil from the contact area with the onset of sliding and hence increasing asperities' contact on the mated surfaces. The friction coefficient increases until the resistance to stick owing to grooving, asperity interlocking, and/or adhesive junctions, as well as material transfer is overcome, and slip occurs.

5. Conclusions

The results of the experimental investigation demonstrate that the coefficient of friction of steel/shale pairs decreases exponentially from static to dynamic friction coefficient with increasing sliding displacement. The difference between static and dynamic friction coefficients and the critical distance D_c under the dry friction condition is much larger than that under the lubricated condition. The transition from static to dynamic friction coefficient is greatly affected by the normal load, quiescent time, and sliding velocity, especially the lubricating condition. Maintaining continuous lubrication of the contact area by the lubricant is crucial to reduce or eliminate the stick-slip motion. Static and kinetic frictions are determined by destroying the surface natural oxide film of steel and the skin layer asperities of shale, microgrooving owing to protruding carbides of the steel and mineral of the shale forming or breaking, respectively, of adhesive junctions. The change laws of friction of stick-slip motion between steel and shale and the empirical formula of friction coefficient fitting from the experimental data in this study provide an insight into the transition from static to dynamic friction of steel/shale pairs and have tremendous guiding significance in the accurate value of friction force between the drill string and borehole wall under the sliding drilling condition, which is the key to realize intelligent drilling.

Data Availability

The data used to support the findings of this study are available within the article.

Conflicts of Interest

The authors declare that they have no conflicts of interest.

Acknowledgments

The authors gratefully acknowledge the financial support of the Major Science and Technology Innovation Project of Shandong Province (Grant no. 2019JZZY010446) and the Fundamental Research Funds for the Central Universities (Grant no. 20CX02322A).

References

[1] C. Gillan, S. G. Boone, M. G. Leblanc, R. P. Picard, and R. T. Fox, "Applying computer based precision drill pipe rotation and oscillation to automate slide drilling steering control," in *Proceedings of the Canadian Unconventional Resources Conference*, p. 11, 2011.

[2] N. R. Zwarich, A. R. McSpadden, M. A. Goodman, R. Trevisan, and R. F. Mitchell, "Application of a new dynamic tubular stress model with friction," in *Proceedings of the IADC/SPE Drilling Conference and Exhibition*, p. 19, 2018.

[3] M. Abughaban, A. Alshaarawi, C. Meng, G. Ji, and W. Guo, "Optimization of drilling performance based on an intelligent drilling advisory system," in *Proceedings of the International Petroleum Technology Conference*, p. 17, Beijing, China, 2019.

[4] N. D. J. P. T. Spencer, "Sliding friction: physical principles and applications," *Physics Today*, vol. 52, pp. 66–68, 1999.

[5] H. Olsson and K. J. Astrom, "Friction generated limit cycles," *IEEE Transactions on Control Systems Technology*, vol. 9, no. 4, pp. 629–636, 2001.

[6] E. J. Berger and T. J. Mackin, "On the walking stick-slip problem," *Tribology International*, vol. 75, pp. 51–60, 2014.

[7] P. E. Rossouw, L. S. Kamelchuk, and R. P. Kusy, "A fundamental review of variables associated with low velocity frictional dynamics," *Seminars in Orthodontics*, vol. 9, no. 4, pp. 223–235, 2003.

[8] K. Nakano, "Two dimensionless parameters controlling the occurrence of stick-slip motion in a 1-DOF system with Coulomb friction," *Tribology Letters*, vol. 24, no. 2, pp. 91–98, 2006.

[9] K. Nakano and S. Maegawa, "Stick-slip in sliding systems with tangential contact compliance," *Tribology International*, vol. 42, no. 11-12, pp. 1771–1780, 2009.

[10] C. A. Brockley and H. R. Davis, "The time-dependence of static friction," *Journal of Tribology*, vol. 12, pp. 35–41, 1968.

[11] J. E. Dunkin and D. E. Kim, "Measurement of static friction coefficient between flat surfaces," *Wear*, vol. 193, no. 2, pp. 186–192, 1996.

[12] J. F. Ferrero and J. J. Barrau, "Study of dry friction under small displacements and near-zero sliding velocity," *Wear*, vol. 209, no. 1-2, pp. 322–327, 1997.

[13] T. Baumberger, P. Berthoud, and C. Caroli, "Physical analysis of the state- and rate-dependent friction law. II. Dynamic friction," *Physical Review B*, vol. 60, no. 6, pp. 3928–3939, 1999.

[14] M. Eriten, A. A. Polycarpou, and L. A. Bergman, "A physics-based friction model and integration to a simple dynamical system," *Journal of Vibration and Acoustics*, vol. 134, 2012.

[15] M. Eriten, "Multiscale physics-based modeling of friction," *Dissertations & Theses Gradworks.*, 2012.

[16] M. Eriten, A. A. Polycarpou, and L. A. Bergman, "Physics-based modeling for fretting behavior of nominally flat rough surfaces," *International Journal of Solids and Structures*, vol. 48, no. 10, pp. 1436–1450, 2011.

[17] B. Bhushan, "Contact mechanics of rough surfaces in tribology: multiple asperity contact," *Tribology Letters*, vol. 4, pp. 1–35, 1998.

[18] U. Andreaus and P. Casini, "Dynamics OF friction oscillators excited BY a moving base and/or driving force," *Journal of Sound and Vibration*, vol. 245, no. 4, pp. 685–699, 2001.

[19] J. Awrejcewicz and P. Olejnik, "Analysis of dynamic systems with various friction laws," *Applied Mechanics Reviews*, vol. 58, no. 6, pp. 389–411, 2005.

[20] J. Swevers, F. Al-Bender, C. G. Ganseman, and T. Projogo, "An integrated friction model structure with improved presliding behavior for accurate friction compensation," *IEEE Transactions on Automatic Control*, vol. 45, no. 4, pp. 675–686, 2000.

[21] W. Jerzy, S. Andrzej, W. Marian, T. Kapitaniak, and A. Stefa Ski, "Hysteretic effects of dry friction: modelling and experimental studies," *Philosophical Transactions of the Royal Society A Mathematical Physical & Engineering Sciences*, vol. 366, pp. 747–765, 2008.

[22] A. Ruina, "Slip instability and state variable friction laws," *Journal of Geophysical Research: Solid Earth*, vol. 88, no. B12, pp. 10359–10370, 1983.

[23] C. Canudas de Wit, H. Olsson, K. J. Astrom, and P. Lischinsky, "A new model for control of systems with friction," *IEEE Transactions on Automatic Control*, vol. 40, no. 3, pp. 419–425, 1995.

[24] P. Dupont, V. Hayward, B. Armstrong, and F. Altpeter, "Single state elastoplastic friction models," *IEEE Transactions on Automatic Control*, vol. 47, no. 5, pp. 787–792, 2002.

[25] P. Dahl, *A Solid Friction Model*, p. 31, Aerospace Cooperation, El Segundo, CA, USA, 1968.

[26] J. H. Dieterich, "Time-Dependent friction in rocks," *Journal of Geophysical Research*, vol. 77, no. 20, pp. 3690–3697, 1972.

[27] J. H. Dieterich, "Modeling of rock friction: 2. Simulation of preseismic slip," *Journal of Geophysical Research*, vol. 84, no. B5, pp. 2169–2175, 1979.

[28] J. H. Dieterich, "Time-dependent friction and the mechanics of stick-slip," *Pure and Applied Geophysics PAGEOPH*, vol. 116, no. 4-5, pp. 790–806, 1978.

[29] N. M. Beeler, T. Tullis, and J. D. Weeks, "The roles of time and displacement in the evolution effect in rock friction," *Geophysical Research Letters*, vol. 21, 1994.

[30] T. Baumberger and C. Hiver, "Physical analysis of the state- and rate-dependent friction law: static friction," *Physical Review B: Condensed Matter*, vol. 59, 1999.

[31] J. Rice and A. Ruina, "Stability of steady frictional slipping," *Journal of Applied Mechanics-transactions of The Asme - J APPL MECH*.vol. 50, 1983.

[32] W. Xueying, H. Ni, R. Wang, L. Zhang, and P. Wang, "Drag-reduction and resonance problems of a jointed drillstring in the presence of an axial excitation tool," *Journal of Energy Resources Technology*, vol. 141, Article ID 032904, 2019.

[33] P. Wang, H. Ni, W. Xueying, and R. Wang, "Modelling the load transfer and tool surface for friction reduction drilling by vibrating drill-string," *Journal of Petroleum Science and Engineering*, vol. 164, 2018.

[34] M. Sarker, D. G. Rideout, and S. D. Butt, "Dynamic model for longitudinal and torsional motions of a horizontal oilwell drillstring with wellbore stick-slip friction," *Journal of Petroleum Science and Engineering*, vol. 150, pp. 272–287, 2017.

[35] E. Rabinowicz, "The nature of the static and kinetic coefficients of friction," *Journal of Applied Physics*, vol. 22, no. 11, pp. 1373–1379, 1951.

[36] B. Mendez and R. Miguel, "Transition from the static to the kinetic coefficient of friction," 2020.

[37] E. K. Mitchell, Y. Fialko, and K. M. J. G. G. G. Brown, "Frictional properties of gabbro at conditions corresponding to slow slip events in subduction zones," *Geochemistry Geophysics Geosystems*, vol. 16, 2015.

[38] K. Tian, Z. Li, N. N. Gosvami, D. L. Goldsby, and R. W. C. J. A. Nano, "The memory distance for interfacial chemical bond-induced friction at the nanoscale," vol. 13, 2019.

[39] Q. Li, T. E. Tullis, D. Goldsby, and R. W. Carpick, "Frictional ageing from interfacial bonding and the origins of rate and state friction," *Nature*, vol. 480, no. 7376, pp. 233–236, 2011.

[40] P. Wang, H. Ni, R. Wang, Z. Li, and Y. Wang, "Experimental investigation of the effect of in-plane vibrations on friction for different materials," *Tribology International*, vol. 99, pp. 237–247, 2016.

[41] D. J. Whitehouse, "Surface topography and quality and its relevance to wear," in *proceedings of the Fundamentals of Tribology*, pp. 17–52, Massachusetts Institute of Technology, Cambridge, MA, USA, 1978.

[42] X. Shi, S. Jiang, S. Lu et al., "Investigation of mechanical properties of bedded shale by nanoindentation tests: a case study on Lower Silurian Longmaxi Formation of Youyang area in southeast Chongqing, China," *Petroleum Exploration and Development*, vol. 46, no. 1, pp. 163–172, 2019.

[43] K. Jankowski, A. Saha, and A. Stefański, "Introduction of novel model of friction and analysis of presliding domain of friction with non-local memory effect based upon Maxwell slip model structures," *Tribology International*, vol. 102, pp. 378–391, 2016.